



# 1 A Novel Objective Function DYNO for Automatic Multi- 2 variable Calibration and Application to Assess Effects of 3 Velocity versus Temperature Data for 3D Lake Models 4 Calibration

5 Wei Xia<sup>1,2,3</sup>, Taimoor Akhtar<sup>4</sup>, Christine A. Shoemaker<sup>1,2,3</sup>

6 <sup>1</sup>Department of Civil and Environmental Engineering, National University of Singapore, 117576, Singapore

7 <sup>2</sup>Department of Industrial Systems Engineering and Management, National University of Singapore, 117576,  
8 Singapore

9 <sup>3</sup>Energy and Environmental Sustainability for Megacities (E2S2) Phase II, Campus for Research Excellence and  
10 Technological Enterprise (CREATE), 138602, Singapore

11 <sup>4</sup>RWDI Consulting Engineers and Scientists, N1G 4P6, ON, Canada

12 *Correspondence to:* Wei Xia (xiawei@u.nus.edu)

13 **Abstract.** This study introduced a novel Dynamically Normalized objective function (DYNO) for multi-variable  
14 (i.e., temperature and velocity) model calibration problems. DYNO combines the error metrics of multiple  
15 variables into a single objective function by dynamically normalizing each variable's error terms using information  
16 available during the search. DYNO is proposed to dynamically adjust the weight of the error of each variable  
17 hence balancing the calibration to each variable during optimization search. The DYNO is applied to calibrate a  
18 tropical hydrodynamic model where temperature and velocity observation data are used for model calibration  
19 simultaneously. We also investigated the efficiency of DYNO by comparing the result of using DYNO to results  
20 of calibrating to either temperature or velocity observation only. The result indicates that DYNO can balance the  
21 calibration in terms of water temperature and velocity and that calibrating to only one variable (e.g., temperature  
22 or velocity) cannot guarantee the goodness-of-fit of another variable (e.g., velocity or temperature). Our study  
23 suggested that both temperature and velocity measures should be used for hydrodynamic model calibration in real  
24 practice. Our example problems were computed with a parallel optimization method PODS but DYNO can also  
25 be easily used in serial applications.

## 26 1. Introduction

27 Hydrodynamic models simulate the hydrodynamic and thermodynamic processes in lakes and reservoirs that are  
28 important for simulating water quality in aquatic eco-systems (Chanudet et al., 2012). These simulation models  
29 (e.g., hydrodynamic modelling) play a critical role in managing water bodies (e.g., rivers, lakes, and coastal areas),  
30 as they are built to simulate the spatial and temporal distributions of specific water quality variables, and to study  
31 the response of a water body to different future management scenarios. The parameters of these models usually  
32 need to be calibrated to measured data to adequately represent local effects and hydrodynamic processes. Model  
33 calibration is a vital step in complex hydrodynamic modelling of lakes and other aquatic systems.

34 Model calibration of hydrodynamic models is mainly done manually (also called trial and error), where  
35 experts tune the parameters and simultaneously evaluate the goodness-of-fit between the simulation output and  
36 observations. This process is subjective, time-intensive and requires extensive expert knowledge (Afshar et al.,  
37 2011; Xia et al., 2021; Solomatine et al., 1999; Fabio et al., 2010; Baracchini et al., 2020). The challenges



38 associated with manual calibration have encouraged the application of auto-calibration to hydrodynamic models,  
39 where the calibration is set up as an inverse problem to minimize the error between the simulation and  
40 observations. Some studies (e.g., Gaudard et al. (2017), Luo et al. (2018), Ayala et al. (2020) and Wilson et al.  
41 (2020)) have applied automatic calibration to one-dimensional hydrodynamic lake models where water  
42 temperature is the variable that is simulated and calibrated. These one-dimensional models are relatively cheap to  
43 run, allowing the use of automatic calibration methods that typically require many simulation evaluations to  
44 determine suitable parameter sets (e.g., differential evolution used in Luo et al. (2018) and Monte Carlo sampling  
45 used in Ayala et al. (2020)). However, one-dimensional models are unable to simulate the spatial distribution of  
46 some water variables, and thus may not be suitable for certain studies. Consequently, 2-dimensional or 3-  
47 dimensional models are preferred for studying the spatial-temporal distribution of water variables and are  
48 increasingly used to study lakes around the world (Chanudet et al., 2012; Galelli et al., 2015; Hui et al., 2018;  
49 Soullignac et al., 2017; Wahl and Peeters, 2014; Xu et al., 2017; Baracchini et al., 2020) . The calibration of 3-  
50 dimensional models, though, is considerably more challenging than calibration of one-dimensional models, since  
51 3-dimensional models are significantly more computationally expensive and also involve more complicated  
52 physical processes (such as advection of flows).

53 The computationally expensive character of 3-dimensional models makes traditional optimization  
54 methods, such as differential evolution and Monte Carlo sampling, unsuitable for automatic calibration because  
55 these methods usually require many evaluations to get an acceptable solution. Surrogate-based optimization is  
56 highly suitable for such problems (Bartz-Beielstein and Zaefferer, 2017; Lu et al., 2018; Razavi et al., 2012) and  
57 recent studies have applied surrogate-based optimization methods to parameter estimation of hydrodynamics  
58 models. Surrogate-based optimization methods use a cheap-to-run surrogate approximation model (of the  
59 calibration objective) fitted with all known (i.e., already evaluated) values of the original expensive objective  
60 function, to guide the optimization search and reduce the number of evaluations required on the expensive  
61 simulations. For example, Xia et al. (2021) proposed a new optimization method called PODS (parallel  
62 optimization with dynamic coordinate search using surrogates) suitable for computationally expensive problems,  
63 and applied it to automatic calibration of a three-dimensional lake hydrodynamic models. More elaborate  
64 discussions on surrogate-based optimization algorithms can be found in Xia et al. (2021), Xia and Shoemaker  
65 (2021), Razavi et al. (2012), Bartz-Beielstein and Zaefferer (2017) and Haftka et al. (2016).

66 Computational intensity is not the only critical challenge associated with parameter estimation of 3-  
67 dimensional hydrodynamic models. Parameter estimation of these models is also a multi-site & multi-variable  
68 calibration problem, i.e., observation data is usually available at multiple locations and the underlying models  
69 simulate multiple variables (e.g., temperature and velocity). Moreover, simultaneous calibration of multiple  
70 variables is desired due to complex interactions between the different variables. For instance, temperature and  
71 velocity are inter-dependent variables of a lake hydrodynamic model, since water temperature affects the  
72 movement of water, and water velocity affects the distribution of water temperature. However, most prior research  
73 studies have calibrated hydrodynamic models to only temperature. This might because temperature measurements  
74 are relatively less expensive to get compared with velocity measurements and often temperature measurements  
75 are available to help predict water quality phenomenon. Wahl and Peeters (2014) use the measured water  
76 temperatures to calibrate a 3-dimensional hydrodynamic model of Lake Constance. Kaçikoç and Beyhan (2014)  
77 calibrate the temperature of Lake Egirdir hydrodynamic model, the flow simulation of which is used for the lake



78 water quality modeling. Marti et al. (2011) and Xue et al. (2015) also only used temperature data for lake  
79 hydrodynamic model calibration. Moreover, these studies use manual calibration for parameter estimation. Xia et  
80 al. (2021) use automatic calibration for parameter estimation, but only use water temperature observations in the  
81 calibration process. Reproducing water level is also a parameter estimation approach that pseudo-considers flow  
82 dynamics in calibration; however, a calibrated model that correctly simulates observed water level does not  
83 necessarily reproduce the observed 3D flow field accurately (Wagner and Mueller, 2002; Parsapour-Moghaddam  
84 and Rennie, 2018).

85 Hydrodynamics models predict the velocities throughout the water body. These results are important to  
86 understand the spatial distribution of water quality problems in sizeable lakes. For the purposes of model  
87 calibration it is useful to know whether efforts to measuring velocity directly are justifiable if temperature data is  
88 already available. We will examine the extent to which direct measurement of velocities justify the extra effort by  
89 giving more accurate results for hydrodynamics models and also look at the error associated with calibrating (for  
90 hydrodynamics) to temperature only, which is rarely studied in literature.

91 There are a few studies that attempt to calibrate hydrodynamic models to both temperature and velocity.  
92 Chanudet et al. (2012) attempt to calibrate both temperature and velocity sequentially (using manual calibration),  
93 i.e., they calibrate water temperature first and then the current velocities. Baracchini et al. (2020) performed two  
94 sequential steps in the automatic calibration of temperature and velocity, and the velocity calibration is based on  
95 the results obtained from temperature calibration. However, one problem with such two-step sequential  
96 approaches, either by manual or auto-calibration is that the calibration of the second variable might significantly  
97 alter the calibration quality of the first variable. This is especially true for multi-variable calibration problems,  
98 where the multiple variables being calibrated are sensitive to the parameters being calibrated. Other examples of  
99 such multi-variable calibration problems include watershed model calibration (Franco et al., 2020) and seawater  
100 intrusion model calibration (Coulon et al., 2021) etc. These multi-variable problems desire calibration frameworks  
101 that allow simultaneous calibration of all variables rather than calibrating one and then the second.

102 There are prior studies that simultaneously calibrate both temperature and velocity variables of  
103 hydrodynamic models. However, these use a trial and error (manual) mechanism for calibration (Râman Vinnâ et  
104 al., 2017; Soullignac et al., 2017; Jin et al., 2000; Paturi et al., 2014). Manual calibration of multiple hydrodynamic  
105 variables simultaneously, is even harder than calibration of a single variable. A key challenge for automatic  
106 calibration of multi-variable calibration problems is in defining a suitable objective function to calibrate multiple  
107 variables simultaneously. Traditional approaches using automatic methods typically formulate the goodness-of-  
108 fit of multiple variables into a single objective function by adding weights between the goodness-of-fit of multiple  
109 variables (Afshar et al., 2011; Pelletier et al., 2006). However, a drawback of this approach is that the relative  
110 error magnitude of each variable of the new solutions found will probably varying during the search making it  
111 difficult to determine appropriate weights since they need to be determined / defined *a priori*, i.e., before  
112 optimization.

113 Another approach for calibration of multi-variables is using multi-objective optimization techniques  
114 (Afshar et al., 2013). However, multi-objective techniques are commonly used to optimize multiple sub-objectives  
115 that have a trade-off between each sub-objective (Akhtar and Shoemaker, 2016; Reed et al., 2013; Alfonso et al.,  
116 2010; Giuliani et al., 2016; Herman et al., 2014). While for the multi-variable hydrodynamic calibration problems,  
117 it is not apparent that there is usually a trade-off between the fit of multiple variables. Moreover, Multi-Objective



118 Optimization (MOO) is considerably more computationally difficult than Single Objective Optimization (SOO)  
 119 and typically requires many more objective function evaluations. Thus, MOO may not be desired for  
 120 computationally expensive calibration problems, especially when a significant trade-off between the objectives  
 121 may not be present. Consequently, multi-variable calibration utilizing efficient SOO algorithms, while balancing  
 122 the calibration to each variable equally during calibration, is a research area of significant value.

123 We introduce a new Dynamically Normalized Objective Function (DYNO) for automatic multi-variable  
 124 calibration problem. The error of each variable (e.g., temperature and velocity of hydrodynamic models) is  
 125 dynamically normalized by using the information about variable error of the evaluations found during the  
 126 optimization search process. In this way, the balance between calibration of each variable is dynamically adjusted.  
 127 We tested the efficiency of DYNO on a computationally expensive hydrodynamic lake model of a tropical  
 128 reservoir, which takes 5 hours to run per simulation. DYNO is coupled into a recent parallel surrogate optimization  
 129 algorithms PODS (Xia et al., 2021) and successfully applied for the calibration of multiple variables of the  
 130 hydrodynamic model. Using DYNO, we investigate the impact of using temperature and/or velocity observations  
 131 on model accuracy.

## 132 2. Methodology

### 133 2.1 Multi-variable Calibration Problems Description

134 The calibration problems investigated in this study are multi-site (i.e., observations are available from multiple  
 135 locations), multi-variable (e.g., temperature and velocity for hydrodynamics) problems, and are defined,  
 136 mathematically, as follows (the variable and function definition are given in Table 1):

$$137 \min_{\mathbf{X} \in \Theta} F(\mathbf{X}|\mathbf{K}) = F(\{f_k(\mathbf{X})|k \in \mathbf{K}\}) \quad (1)$$

$$138 f_k(\mathbf{X}) = f_k(\{g_j(\text{sim}_j^k(\mathbf{X}), \text{obs}_j^k)|j = 1, \dots, M\}) \quad (2)$$

139 Note that the notation  $\{z_i\}$  in Eq. (2) is simply meant to imply the function on the left depends on the finite series  
 140 of quantities inside the braces  $\{\bullet\}$ .

141 **Table 1.** Notation and definitions of variables and functions in Eq. (1) and (2).

Variable	Description
$\mathbf{K}$	The set of variables the observation data of which is used in calibration. For example, $\mathbf{K} = [\text{Tem}]$ means that water temperature observation is used for calibration, i.e., water temperature is the variable that is being calibrated; $\mathbf{K} = [\overline{\text{Vel}}]$ means velocity observation is used for calibration; $\mathbf{K} = [\text{Tem}, \overline{\text{Vel}}]$ means that both temperature and velocity observations are used for model calibration
$k$	The symbol for elements in $\mathbf{K}$ variable (e.g., water temperature or velocity, $k = \text{Tem}$ or $k = \overline{\text{Vel}}$ ). $k \in \mathbf{K}$
$\mathbf{X}$	A $d$ dimensional parameter vector restricted to parameter space $\Theta$ , where $d$ is the number of parameters to be optimized
$\Theta$	The parameter space is defined by the upper and lower limits on each parameter ( $\mathbf{X}^{\max}$ and $\mathbf{X}^{\min}$ , respectively)
$M$	The total number of observation locations (or sites).
$j$	The index for observation location. $j = 1, \dots, M$
$\text{Sim}_j^k(\mathbf{X})$	The simulation output of variable $k$ at location $j$ at times $t = 1, \dots, N$ given the parameter vector $\mathbf{X}$
$\text{Obs}_j^k$	The observation (data) of variable $k$ at location $j$ at times $t = 1, \dots, N$



$N$	The total time steps of the observation data
$t$	The index for time steps. $t = 1, \dots, N$
Function	Description
$F(\mathbf{X} \mathbf{K})$	The calibration objective function given the observation data of variables in $K$ for calibration. $F(\mathbf{X} \mathbf{K})$ is a composite function of $f_k(\mathbf{X})$
$f_k(\mathbf{X})$	The error function of variable $k$ over multiple site. $f_k(\mathbf{X})$ is a composite function of $g_j(\text{Sim}_j^k(\mathbf{X}), \text{Obs}_j^k)$ for sites $j = 1, \dots, M$
$g_j(\text{Sim}_j^k(\mathbf{X}), \text{Obs}_j^k)$	Goodness of fit between simulation output $\text{Sim}_j^k(\mathbf{X})$ and observation $\text{Obs}_j^k$ of variable $k$ at location $j$ . When $k = \text{Tem}$ , Normalized Root Mean Square Error (NRMSE) is utilized for $g_j(\bullet)$ . When $k = \overline{\text{Vel}}$ , normalized Fourier Norms of Root Mean Square Error (FNs) is used for $g_j(\bullet)$ .

142

143 The set of parameters  $\mathbf{X}$  being calibrated in this study includes nine parameters ( $d = 9$ ). Details of these  
 144 parameters are provided in Table 2 in section 2.4. The two variables are calibrated in this study are velocity and  
 145 temperature for which data exists for different spatial location and time points.

146 We investigate different calibration formulations, where either one or both of these variables are  
 147 calibrated. Consequently,  $\mathbf{K} = [\text{Tem}]$  means that water temperature observation is used for calibration, i.e., water  
 148 temperature is the variable that is being calibrated;  $\mathbf{K} = [\overline{\text{Vel}}]$  means velocity observation is used for calibration;  
 149  $\mathbf{K} = [\text{Tem}, \overline{\text{Vel}}]$  means that both temperature and velocity observations are used for model calibration, i.e., both  
 150 variables are being calibrated simultaneously. The objective function in each scenario is discussed in section 2.5.

## 151 2.2 DYNO for Model Calibration with Multiple Variables

152 One major issue for model calibration with multiple variables is how to formulate the error of multiple variables  
 153 into a single objective function. In practice, different variables (e.g., temperature and velocity) usually have  
 154 different physical units and magnitudes of error. Their error functions cannot be summed up directly into a single  
 155 objective function if we wish to give the error of each variable an equal weight in the overall objective function.  
 156 The respective error functions have to be normalized. There are goodness-of-fit metrics that can normalize the  
 157 error of different variables (for example Normalized Root Mean Square Error (NRMSE) and Kling-Gupta  
 158 Efficiency (KGE, (Gupta et al., 2009))). However, it is still possible that the highest attainable NRMSE (or KGE)  
 159 value (and the distribution of NRMSE (or KGE) value across the parameter space) for one variable maybe be  
 160 much higher than the highest attainable NRMSE (or KGE) value (and the distribution of NRMSE (or KGE) value)  
 161 of another variable. Hence how to balance such differences among multiple variables is still important even when  
 162 the normalized goodness-of-fit metrics are used.

163 We propose a new general objective function, Dynamically Normalized Objective Function (DYNO),  
 164 for the multi-variable calibration problem (e.g., calibrating temperature and velocity simultaneously). DYNO (as  
 165 shown in Eq. (3)) normalizes the error of each variable  $f_k(\mathbf{X})$  with its upper and lower bound,  $f_k^{\max}$  and  $f_k^{\min}$  of  
 166 all evaluations found so far  $\boldsymbol{\psi}$ . Since true values of bounds are not known,  $f_k^{\max}$  and  $f_k^{\min}$  are dynamically updated  
 167 during the optimization search after each iteration. Mathematical formulation of the multi-variable calibration  
 168 problem, with the Dynamically Normalized Objective Function, is as follows:

$$169 \min F(\mathbf{X}|\mathbf{K}) = \sum_{k \in K} \frac{f_k(\mathbf{X}) - f_k^{\min}(\mathbf{X})}{f_k^{\max}(\mathbf{X}) - f_k^{\min}(\mathbf{X})} \quad (3)$$



170  $f_k^{max}(\mathbf{X}) = \max \{f_k(\mathbf{X}) \text{ for all } \mathbf{X} \in \boldsymbol{\psi}\}$  (4)

171  $f_k^{min}(\mathbf{X}) = \min \{f_k(\mathbf{X}) \text{ for all } \mathbf{X} \in \boldsymbol{\psi}\}$  (5)

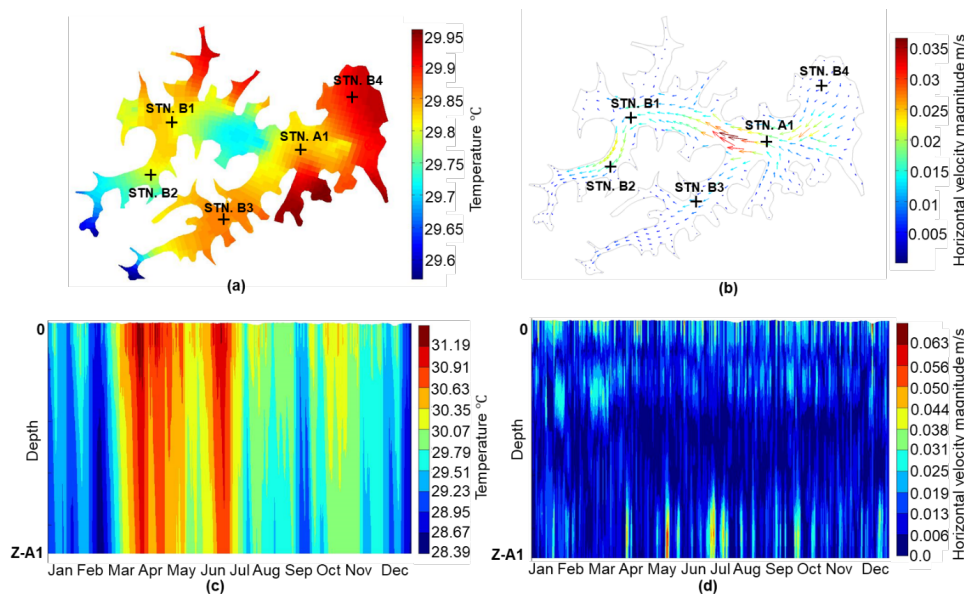
172 where  $f_k^{max}(\mathbf{X})$  and  $f_k^{min}(\mathbf{X})$  are the maximum and minimum values of  $f_k(\mathbf{X})$  for all evaluation in  $\boldsymbol{\psi}$ , which is a  
173 set of all the evaluations evaluated so far and hence they have to be updated dynamically in each iteration during  
174 optimization. The detailed description of the implementation of Eq. (3) in the algorithm (i.e., PODS) tested in this  
175 study is given in Section 2.6 (the Algorithm Description section).

### 176 2.3 Study Site and Data

177 We use a 3-dimensional model of a tropical reservoir as an example to test the efficiency of DYN0 for multi-  
178 variable calibration problems and to study the impact of using temperature and/or velocity data for model  
179 calibration. The horizontal boundary of the studied reservoir is given in Fig. 1 (a) and (b). One online water quality  
180 profiler station (STN. A1) was installed in the middle of the reservoir. The water temperature data at the station  
181 are available at various depths. The measured temperature data is used for model calibration in a previous study  
182 (Xia et al., 2021). We use this calibrated model to create synthetic observation data since the real velocity  
183 measurements are not available. We first assume a set of “true” model parameters  $\mathbf{X}^R$ . The value of  $\mathbf{X}^R$  is based  
184 on an expert’s guess and is listed in Table 2. The spatial and temporal observation data for the hypothetical lake  
185 is synthetically generated based on the “true” model parameters  $\mathbf{X}^R$ . The synthetic observation data for the  
186 hypothetical temperate lake is generated by running the simulation model for one year with a vector of model  
187 parameters  $\mathbf{X}^R$ . The simulation output is then saved hourly in  $N$  time steps for multiple variables, i.e., temperature  
188 and velocity ( $\mathbf{K} = [Tem, \overline{Vel}]$ ) at  $M$  locations (specified in Fig. 1). In our study case,  $N = 8761$  and  $M = 12$   
189 with different depths of five hypothetical sensor stations (STN. A1 and STN. B1-4 as shown in Fig. 1 (a) and (b)).

190 The saved hourly simulated output time series is denoted as  $\Gamma = \{Sim^k(\mathbf{X}^R), k \in \mathbf{K} = [Tem, \overline{Vel}]\}$ ,  
191 which as defined (in Table 1) contains information for each time step,  $t = 1, \dots, N$ . So  $\Gamma$  is used as observation  
192 data for model calibration, i.e.,  $Obs^k, k \in \mathbf{K} = [Tem, \overline{Vel}]$  in Eq. (1). In the test of optimization for calibration,  
193 the true value of the parameter vector  $\mathbf{X}^R$  is not provided to the optimization. The optimization will, instead, search  
194 for a best value of  $\mathbf{X}$  that will minimize objective function  $F(\mathbf{X}|\mathbf{K})$ , where  $\mathbf{K} = [Tem], [\overline{Vel}], \text{ or } [Tem, \overline{Vel}]$ . So  
195 the goal of automatic calibration via optimization is to obtain an optimum calibration  $\mathbf{X}^*$  that results in simulation  
196 model output,  $Sim^k(\mathbf{X}), k \in \mathbf{K}$ , (see Eq. (1) and Eq. (2)) that is close to the synthetical observation time series  
197 data in  $\Gamma$ .

198 The temperature and velocity simulation results based on the “true” model parameters (shown in Table  
199 2) show temporal and spatial variation, as shown in Fig. 1 (a)-(d). Figure 1 (a) and (b) show the temperature and  
200 horizontal velocity distribution at the surface layer. Figure 1 (c) and (d) show the distribution of temperature and  
201 velocity magnitude at STN. A1. There is obvious temperature stratification in the vertical direction (as shown in  
202 Fig. 1(c)). We have the sampling locations across the reservoir where the observations can be used to calibrate  
203 the model parameters.



204

205 **Figure 1.** (a) Simulated (with “true” model parameters) temperature spatial distribution with sampling locations.  
206 (b) Simulated velocity spatial distribution with sampling locations. (c) Time-depth plot of simulated temperature  
207 at STN. A1. (d) Time-depth plot of velocity magnitude at STN. A1. Z-A1 is the maximum water depth at station  
208 A1.

#### 209 2.4 Hydrodynamic Model and Calibration Parameters

210 The description of the hydrodynamic model is given in Xia et al., (2021). The hydrodynamic model is built with  
211 Delft3D-FLOW (Hydraulics, 2006). The Delft3D-Flow hydrodynamic model used was set up by the water  
212 utilities’ employees and consultants, including the domain construction, input data preparation, and model  
213 configuration. The grid coordinate system is based on Cartesian coordinates (Z-grid), which has horizontal co-  
214 ordinate lines that are almost parallel with density interfaces to reduce artificial mixing of scalar properties such  
215 as temperature. The number of grid points in the x-direction is 65, the number of grid points in the y-direction is  
216 67, and the number of layers in vertical is 19. A single 1-year simulation takes about 5 hours to run in serial on a  
217 windows desktop with CPU Intel Core i7-4790.

218 There are nine tunable model parameters (listed in Table 2) in the model. The first five parameters in  
219 Table 2 are related to the turbulence calculation. The k-ε closure model (Uittenbogaard et al., 1992) was chosen  
220 as the turbulence closure model to calculate the viscosity and diffusivity of the water. The calculation of the  
221 viscosity and diffusivity involves five parameters: 1) background viscosity in horizontal  $v_H^{back}$ , 2) vertical  $v_V^{back}$ ,  
222 3) the background eddy diffusivity in horizontal  $D_H^{back}$ , 4) vertical  $D_V^{back}$  and 5) the Ozmidov length  $L_{oz}$ . These  
223 parameters affect both the velocity and the temperature. The vertical exchange of horizontal momentum and mass  
224 is affected by vertical eddy viscosity and eddy diffusivity coefficient (Elhakeem et al., 2015). The horizontal  
225 velocities are affected by the horizontal eddy viscosity and diffusivity coefficients (Chanudet et al., 2012).  
226 Chanudet et al. (2012) highlighted that the most impactful parameter for temperature is the background vertical  
227 eddy viscosity and the Ozmidov length  $L_{oz}$  also has a significant effect on the thermal stratification by affecting  
228 the vertical temperature mixing. The bottom roughness, which has a direct impact on velocity, is computed





229 according to Manning formulation with Manning's coefficient ( $n$ ) given, which is a parameter that also should be  
 230 calibrated.

231 The next three parameters in Table 2 are related to the simulation of surface heat flux. In the heat flux  
 232 model, the evaporative heat flux and heat convection by forced convection is parameterized by the Dalton number  
 233  $c_e$  and Stanton number  $c_H$ , respectively, which are also in the list of calibration parameters. The Secchi depth  
 234  $H_{Secchi}$  (also included in Table 2) is another parameter required by the Ocean heat flux model. Secchi depth is  
 235 related to the transmission of radiation in deeper water and thus affects the vertical distribution of heat in the water  
 236 column (Chanudet et al., 2012). Heat fluxes through the reservoir bottom were not simulated in the current model.  
 237 The last parameter is the manning coefficient, which affects the roughness of the bottom of the lake.

238 All these nine parameters affect (either directly or indirectly) the thermal and current activity in the water  
 239 body, and thus, are included in the calibration process. The calibration range for these parameters (given in Table  
 240 2) is suggested by Singapore water utilities employees and consultants.

241 **Table 2.** Model parameter used in calibration.  $X^R$  denotes the true solution used to generate synthetical  
 242 temperature and velocity observations at multi-sites.

Parameter vector $X$	Parameter	Description (unit)	Physical process	Range	$X^R$
$x_1$	$v_H^{back}$	Background viscosity in horizontal (m <sup>2</sup> /s)	3D turbulence	0.1-1.0 <sup>a,b,d,e</sup>	0.5
$x_2$	$D_H^{back}$	Background eddy diffusivity in horizontal (m <sup>2</sup> /s)		0.1-1.0 <sup>a,b,d,e</sup>	0.5
$x_3$	$v_V^{back}$	Background viscosity in vertical (m <sup>2</sup> /s)		0-0.005 <sup>a,b,c,e</sup>	5.00E-05
$x_4$	$D_V^{back}$	Background eddy diffusivity in vertical (m <sup>2</sup> /s)		0-0.005 <sup>a,b,c,e</sup>	5.00E-05
$x_5$	$L_{oz}$	Ozmidov length scale (m)		0-0.05 <sup>a,b,c</sup>	0.015
$x_6$	$H_{Secchi}$	Secchi depth (m)	Heat flux	0.1-2.0 <sup>a,e,f</sup>	1
$x_7$	$c_e$	Dalton number (-)		0.001-0.002 <sup>a,b,c,e</sup>	0.0013
$x_8$	$c_H$	Stanton number (-)		0.001-0.002 <sup>a,b,c,e</sup>	0.0013
$x_9$	$n$	Manning coefficient (m <sup>-1/3</sup> s)	Roughness	0.02-0.03 <sup>a,b,c</sup>	0.022

243 <sup>a</sup>Deltares (2014); <sup>b</sup>Chanudet et al. (2012); <sup>c</sup>Wahl and Peeters (2014); <sup>d</sup>Råman Vinnå et al. (2017); <sup>e</sup>Soullignac et  
 244 al. (2017); <sup>f</sup>Pijcke (2014)  
 245

## 246 2.5 Calibration Problem Formulation

247 Three scenarios are considered to investigate the impact of model calibration against temperature and/or velocity  
 248 observations: 1) calibrating to temperature data only (Cali-Tem), 2) calibrating to velocity data only (Cali-Vel),  
 249 and 3) calibrating to both temperature and velocity together (Cali-Both). This corresponds to optimizing the  
 250 problem  $F(X|K)$  in Eq. (1), where  $K = [Tem]$ ,  $[\overline{Vel}]$ , and  $[Tem, \overline{Vel}]$  respectively for the three scenarios. The  
 251 first two scenarios calibrate to only one variable, and the last scenario calibrates both variables simultaneously.

### 252 2.5.1 Model Calibration with One Variable

253 The objective functions for Cali-Tem and Cali-Vel scenarios are summarized in Eq. (6)-(8) and Eq. (9)-(11),  
 254 respectively, where only observations of one variable are included in the calibration.





$$255 \quad F(\mathbf{X}|\mathbf{K} = [Tem]) = f_{Tem}(\mathbf{X}) \quad (6)$$

$$256 \quad f_{Tem}(\mathbf{X}) = \sum_{j=1}^M NRMSE_j^{Tem}(\mathbf{X}) \quad (7)$$

$$257 \quad NRMSE_j^{Tem}(\mathbf{X}) = \frac{\sqrt{\frac{1}{N} \sum_{t=1}^N [Sim_{t,j}^{Tem}(\mathbf{X}) - Obs_{t,j}^{Tem}]^2}}{\frac{1}{N} \sum_{t=1}^N Obs_{t,j}^{Tem}} \quad (8)$$

$$258 \quad F(\mathbf{X}|\mathbf{K} = [\overline{Vel}]) = f_{\overline{Vel}}(\mathbf{X}) \quad (9)$$

$$259 \quad f_{\overline{Vel}}(\mathbf{X}) = \sum_{j=1}^M FNs_j^{\overline{Vel}}(\mathbf{X}) \quad (10)$$

$$260 \quad FNs_j^{\overline{Vel}}(\mathbf{X}) = \frac{\sqrt{\frac{1}{N} \sum_{t=1}^N \|Sim_{t,j}^{\overline{Vel}}(\mathbf{X}) - Obs_{t,j}^{\overline{Vel}}\|_2}}{\sqrt{\frac{1}{N} \sum_{t=1}^N \|Obs_{t,j}^{\overline{Vel}}\|_2}} \quad (11)$$

261 where,  $NRMSE_j^{Tem}(\mathbf{X})$  and  $FNs_j^{\overline{Vel}}(\mathbf{X})$  denote the Normalized Root Mean Square Error (NRMSE) of  
 262 temperature (described in Eq. (8)), and normalized Fourier Norms (FNs) of velocity vectors (described in Eq.  
 263 (11)) at locations  $j$ .  $Sim_{t,j}^{\overline{Vel}}(\mathbf{X})$  and  $Obs_{t,j}^{\overline{Vel}}$  denote the simulated velocity given a parameter vector  $\mathbf{X}$  and observed  
 264 velocity, respectively, at time step  $t$  and location  $j$ .  $Sim_{t,j}^{\overline{Vel}}(\mathbf{X})$  and  $Obs_{t,j}^{\overline{Vel}}$  are 3-dimensional vector.  $\|\cdot\|_2$  in Eq.  
 265 (11) is the Euclidean norm used to quantify the size of a vector.

266 The temperature and velocity data are taken at different depths of multiple stations, and their magnitude  
 267 at different locations might be different due to spatial variation. Hence, the fitness at each location should be  
 268 normalized before being summed into the objective function. For water temperature, Normalized Root Mean  
 269 Square Error (NRMSE, as described in Eq. (8)) is used to quantify and normalize the error between the simulated  
 270 and observed data. For velocity, normalized Fourier Norms of RMSE (FNs, as described in Eq. (11)) are used to  
 271 measure the error between the model-simulated and observed data (corresponding simulated and observed  
 272 velocity data points are three-dimensional vectors). The calculation of the Fourier Norm follows the description  
 273 in Beletsky et al. (2006), Huang et al. (2010), Paturi et al. (2014) and Râman Vinnâ et al. (2017).

## 274 2.5.2 DYNO for Model Calibration with Multiple Variables

275 In the Cali-Both scenario, both temperature and velocity are calibrated simultaneously, which can be treated as a  
 276 bi-objective function problem. The objective function in the Cali-Both scenario (as shown in Eq. (12)) applies the  
 277 DYNO proposed in Eq. (3). The error functions for water temperature, i.e.,  $f_{Tem}(\mathbf{X})$ , and velocity, i.e.,  $f_{\overline{Vel}}(\mathbf{X})$ ,  
 278 are the objective functions of the Cali-Tem scenario (Eq. (7) and the Cali-Vel scenario (Eq. (10), respectively.  
 279 The temperature and velocity errors are dynamically normalized with their upper and lower bounds during the  
 280 search of the optimization algorithm before being summed them into a single objective function. The mathematical  
 281 formulation of the objective function in the Cali-Both Scenario (based on Eq. (3)) is as follows:

$$282 \quad F(\mathbf{X}|\mathbf{K} = [Tem, \overline{Vel}]) = \frac{f_{Tem}(\mathbf{X}) - f_{Tem}^{min}(\mathbf{X})}{f_{Tem}^{max}(\mathbf{X}) - f_{Tem}^{min}(\mathbf{X})} + \frac{f_{\overline{Vel}}(\mathbf{X}) - f_{\overline{Vel}}^{min}(\mathbf{X})}{f_{\overline{Vel}}^{max}(\mathbf{X}) - f_{\overline{Vel}}^{min}(\mathbf{X})} \quad (12)$$

283 where the maximum and minimum of  $f_{Tem}(\mathbf{X})$  and  $f_{\overline{Vel}}(\mathbf{X})$  are updated after each optimization iteration (since  
 284 new parameter sets are sampled in each optimization iteration). As the number of iterations increases, the  
 285 denominators in Eq. (12) also increase since the optimization method finds better minimum objective function  
 286 values. Hence the individual objective function components (for each variable) scale dynamically to maintain a  
 287 roughly equal weight of the terms related to temperature and velocity.



288 As defined in Eq. (6) to Eq. (12), three calibration formulations are investigated in this study. Table 3  
 289 gives a summary of these calibration formulations.

290 **Table 3.** Summary of Objective function formulation for different calibration scenarios.

Scenario Name	Variables used for calibration	Objective Function	Objective Function Formula
Cali-Tem	Temperature	$F(\mathbf{X} \mathbf{K} = [Tem])$	Eq. (6)~(8)
Cali-Vel	Velocity	$F(\mathbf{X} \mathbf{K} = [Vel])$	Eq. (9)~(11)
Cali-Both	Temperature and Velocity	$F(\mathbf{X} \mathbf{K} = [Tem, Vel])$	Eq. (12)

291 **2.6 Optimization Methods**

292 **2.6.1 PODS**

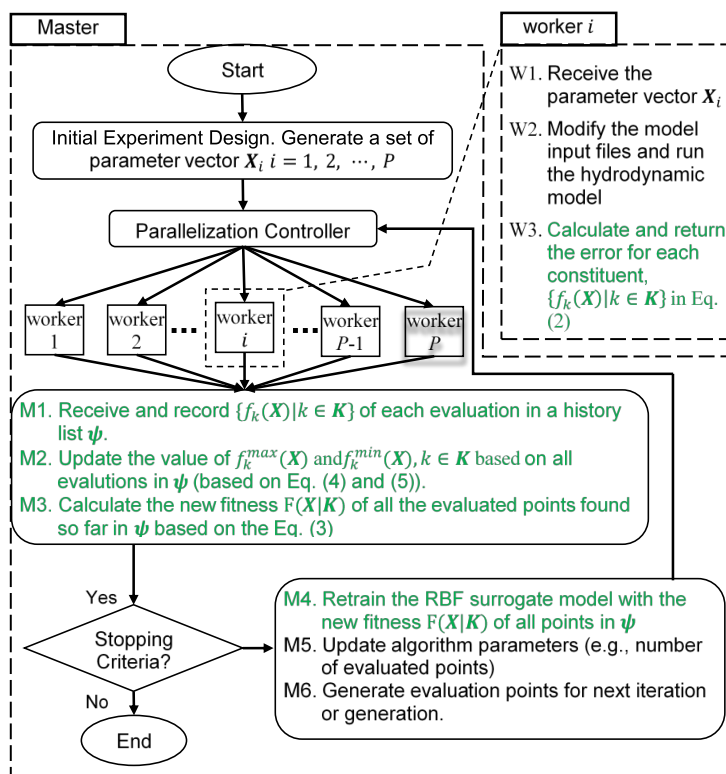
293 We use a new efficient parallel surrogate algorithm PODS (Xia et al., 2021), a synchronous parallel version of  
 294 serial DYCORS introduced by (Regis and Shoemaker, 2013). The serial optimization algorithm, DYCORS, is  
 295 designed for global (with multiple local minima) black-box optimizations problems that are high-dimensional and  
 296 have computationally expensive objectives (Regis and Shoemaker, 2013). Regis and Shoemaker (2013) show that  
 297 serial DYCORS is considerably more efficient than other global optimization methods in obtaining good solutions  
 298 with fewer objective function evaluations, which is very important for expensive objective functions like  
 299 hydrodynamics models (Regis and Shoemaker, 2013). DYCORS uses RBF (Radial Basis Function) surrogates to  
 300 guide the algorithm search towards promising solutions within the solution domain to reduce the number of  
 301 evaluations (Regis and Shoemaker, 2007). Furthermore, DYCORS inherits the dynamic coordinate search idea  
 302 from DDS (Tolson and Shoemaker, 2007) to improve its effectiveness and efficiency for high dimensional  
 303 problems. PODS parallelized the serial DYCORS algorithm by following the general framework of the  
 304 Synchronous Master-Worker Parallel Stochastic RBF Method introduced by Regis and Shoemaker (2009). This  
 305 parallelization strategy of the algorithm allows simultaneous function evaluations on multiple processors (cores)  
 306 in batch mode and can greatly speedup the calibration of computationally expensive models by reducing the  
 307 calibration time and making the calibration of some extremely expensive models computationally tractable.

308 **2.6.2 Implementation of Dynamically Normalized Objective Function in PODS.**

309 The implementation procedure for incorporating the Dynamically Normalized Objective Function into the  
 310 optimization algorithm PODS is described in Fig. 2. In the PODS algorithm, after each iteration, the sampling  
 311 points for the next iteration are generated around the best solution found so far, in terms of the objective function  
 312 value (in Eq. (1)). The use of DYNO affects the selection of the best solution found so far and also the fit of the  
 313 surrogate model. When only one variable is considered in the objective function, the best solution is the evaluation  
 314 with the lowest error between the simulation output and observations of the variable considered. In cases where  
 315 multiple variables are considered in calibration, the best solution should be the evaluation after considering the  
 316 error of multiple variables (as shown in Eq. (3)). Since the maximum and minimum value of the error of each  
 317 variable  $f_k^{max}(\mathbf{X})$  and  $f_k^{min}(\mathbf{X})$  is dynamically changing after new evaluated simulations are available, the  
 318 objective function value in Eq. (3) will be recalculated for all evaluated solutions after each iteration. Hence the  
 319 surrogate model that is an approximation of the real objective function fitted by  $(F(\mathbf{X}|\mathbf{K}), \mathbf{X})$  is also rebuilt with



320 these new objective function values of all evaluated solutions. Refitting of the surrogate model is computationally  
 321 inexpensive compared with the runtime of the expensive objective function. Hence it does not affect overall  
 322 algorithm runtime.



323  
 324 **Figure 2.** Diagram of the implementation of the Dynamic Normalized Objective Function with the parallel  
 325 algorithm PODS.  $P$  is the number of processors available. The green texts (i.e., steps W3, M1-4) are changes  
 326 made on PODS to incorporate DYNO. The rest part follows the original PODS method.

## 327 2.7 Experiments Setup

328 All computational experiments in this study are implemented on a single node on the National Supercomputer  
 329 Center (NSCC) of Singapore, which is a Linux-based platform with dual Intel Xeon E5-2690 v3 Processors, with  
 330 each node having 24 cores. Hence, we set the number of processors  $P$  to be 24. Due to the stochastic nature of the  
 331 optimization algorithm (i.e., PODS) used in this study, multiple optimization runs are executed for each calibration  
 332 experiment in Table 3. Considering that the calibrated hydrodynamic model in this study is extremely expensive,  
 333 we perform three optimization trials for each calibration experiment (see Table 3 for a list of experiments).  
 334 Furthermore, to remove any initial sampling bias, each concurrent optimization trial for the three calibration  
 335 experiments is initialized with the same Latin Hypercube experimental design (so the calibration in each scenario  
 336 is starting from the same initial solutions). We also investigated the performance of different forms of DYNO on  
 337 the Cali-Both scenario (i.e., calibrating to both temperature and velocity data).



338 **3. Numerical Results and Discussion**

339 **3.1 Comparison of Calibrating to Temperature and/or Velocity**

340 **3.1.1 Final Solutions in Goodness-of-fit Metrics**

341 We first compare the three calibration formulations in terms of goodness-of-fit metrics for both temperature and  
 342 velocity. Table 4 summarizes this comparison for the three formulations, i.e., i) Cali-Tem (calibrate temperature  
 343 only), ii) Cali-Vel (calibrate velocity only) and iii) Cali-Both (calibrate temperature and velocity simultaneously)  
 344 (see definition in Table 3), with PODS used as the optimization algorithm and with a budget of 192 simulations.

345 The mean as well as the standard deviation of both temperature error  $f_{Tem}(X^*|K)$  (calculated as Eq. (7))  
 346 and velocity error  $f_{Vel}(X^*|K)$  (Calculated as in Eq. (10)) over three trials are reported in Table 4, for all three  
 347 calibration scenarios.  $X^*$  in Table 4 denotes the optimal calibration solution obtained by PODS in each trial for a  
 348 given scenario (defined by the set of variables  $K$ ). The solution with the lowest variable error ( $f_{Tem}(X^*)$   
 349 or  $f_{Vel}(X^*)$ ) is highlighted in bold in Table 4. Table 4 reports the variable errors of both temperature and velocity  
 350 for all formulations to understand the impact of ignoring or including a variable in the calibration formulation.  
 351 Please note that the temperature error,  $f_{Tem}(X|K = [Tem])$ , reported in Table 4, is exactly the calibration  
 352 objective function in the Cali-Tem scenario ( $F(X|K = [Tem])$ ) as shown in Eq. (7)). Similarly, the velocity error  
 353  $f_{Vel}(X|K = [Tem])$  is exactly the calibration objective function in the Cali-Vel scenario (i.e.,  $F(X|K = [Vel])$ )  
 354 as shown in Eq. (10)). We use the word variable error instead of objective function value when referring to the  
 355 values in Table 4 in subsequent discussions since we are in part looking at the impact of using data from one  
 356 variable to predict another variable for which we don't have data.

357 Table 4 shows that the solution obtained when calibrating to temperature observation only (Cali-Tem)  
 358 has smaller temperature errors but larger velocity errors than that if calibrating to velocity observation data only  
 359 (Cali-Vel). However, it is surprising that when calibrating to both temperature and velocity (Cali-Both), the  
 360 solution obtained by PODS has the lowest temperature and lowest velocity error compared with calibrating to  
 361 either temperature observation or velocity observation only. This might be because calibrating to temperature will  
 362 help to improve the fit of velocity and vice versa. This makes sense because water temperature and velocity are  
 363 two related variables in hydrodynamic modeling, and they are affecting each other. Velocity is the fundamental  
 364 variable of hydrodynamics with directional information not provided by temperature; temperature (via the heat  
 365 flux model) may also affect the velocity field since it affects water density. This might explain calibrating both  
 366 temperature and velocity simultaneously gives the best results.

367 **Table 4.** Summary table of the solution obtained by PODS for each scenario (Cali-Both, Cali-Vel, and Cali-Tem).  
 368  $f_{Tem}(X^*|K)$  and  $f_{Vel}(X^*|K)$  are the temperature error  $f_{Tem}(X^*)$  and velocity error  $f_{Vel}(X^*)$  (calculated in Eq. (7)  
 369 and Eq. (10), respectively, with the optimal solution  $X^*$  obtained in each trial). The mean and standard deviation  
 370 of  $f_{Tem}(X^*|K)$  and  $f_{Vel}(X^*|K)$  among three trials are reported. The variable error is bolded in each scenario when  
 371 the observation of the variable is included in the calibration in each scenario. (Some terms defined in Table 1)

Scenarios	The composite error of each variable (Temperature or Velocity)	
	$f_{Tem}(X^* K)$ Mean (Std.)	$f_{Vel}(X^* K)$ Mean (Std.)
Cali-Both $K = [Tem, Vel]$	<b>0.014 (0.003)</b>	<b>1.939 (0.165)</b>
Cali-Vel $K = [Vel]$	0.087 (0.023)	2.809 (0.319)
Cali-Tem $K = [Tem]$	0.024 (0.005)	5.888 (1.435)



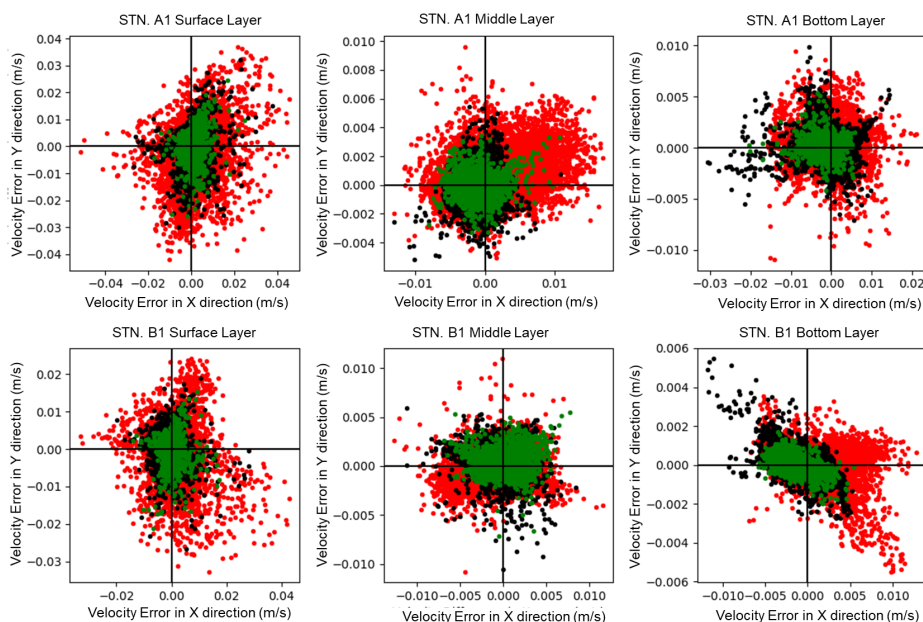
### 372 3.1.2 Visual Comparison of Calibration Errors

373 The above analysis is based on the average variable error statistics only (i.e.,  $f_{Tem}(\mathbf{X}^*|\mathbf{K})$  and  $f_{\overline{Vel}}(\mathbf{X}^*|\mathbf{K})$ ), of the  
374 best results obtained from PODS (over multiple trials) for all calibration scenarios. In order to further analyze the  
375 difference between calibration formulations (in terms of their effectiveness in calibrating both temperature and  
376 velocity), we visually compare the best calibration solutions ( $\mathbf{X}^*$ ) obtained by PODS for each scenario, i.e., Cali-  
377 Tem, Cali-Vel and Cali-Both. We select one representative optimal solution ( $\mathbf{X}^*$ ) from 3 trials in each scenario  
378 for this comparison.

379 The objective function value in terms of temperature and velocity composite error (over multiple  
380 locations) ( $f_{Tem}(\mathbf{X})$  and  $f_{\overline{Vel}}(\mathbf{X})$ ), as formulated in Eq. (7) and (10), respectively) and the corresponding parameter  
381 configuration ( $\mathbf{X}^*$ ) of the selected solution (among three trials) are reported in Table 5. The horizontal velocity  
382 error  $\Delta\overline{Vel}$  (2-dimensional) between simulated velocity  $Sim_{t,j}^{\overline{Vel}}(\mathbf{X}^*)$  and observed velocity  $Obs_{t,j}^{\overline{Vel}}$  (in the  
383 horizontal plane) is plotted as scatter plots of time-series in Fig. 3 (for all calibration scenarios). The temperature  
384 error  $\Delta Tem$  between simulation temperature  $Sim_{t,j}^{Tem}(\mathbf{X}^*)$  and observed temperature  $Obs_{t,j}^{Tem}$  is plotted as a time  
385 series (for each calibration scenario) in Fig. 4.

386 The error plots for the two sampling locations at multiple depths (i.e., surface layers of station STN. A1  
387 and STN. B1 as shown in Fig. 1 (a)) are visualized in Fig. 3 and 4 (for one year). Since the velocity error  $\Delta\overline{Vel}$  at  
388 a particular time and location is a vector (and not a scalar like temperature) and velocity error in 3 dimensions (for  
389 a time-series) is hard to represent visually, Fig. 3 only plots the velocity error (for one year)  $\Delta\overline{Vel}$  in the horizontal  
390 plane (i.e., X and Y directions only). Moreover, each dot represents the error at one point in time within the study  
391 period.

392 Figure 3 plots the difference between the simulated velocity (for the optimized parameter values obtained  
393 from Cali-Tem (red scatter points), Cali-Vel (black scatter points), and Cali-Both (green scatter points) scenarios)  
394 and observed velocity. Ideally, the error for each scatter point should be zero, i.e., at the intersection of the two  
395 lines. Figure 3 illustrates that calibrating to temperature data only (red scatter plot) results in the velocity error  
396  $\Delta\overline{Vel}$  scatter that diverges from the zero velocity error (i.e., the intersection point of the black lines), in comparison  
397 to the corresponding velocity error scatter plots of solutions obtained from calibrating to velocity data only (Cali-  
398 Vel scenario, i.e., black scatter plot) or to both velocity and temperature data (Cali-Both scenario, i.e., green scatter  
399 plot).

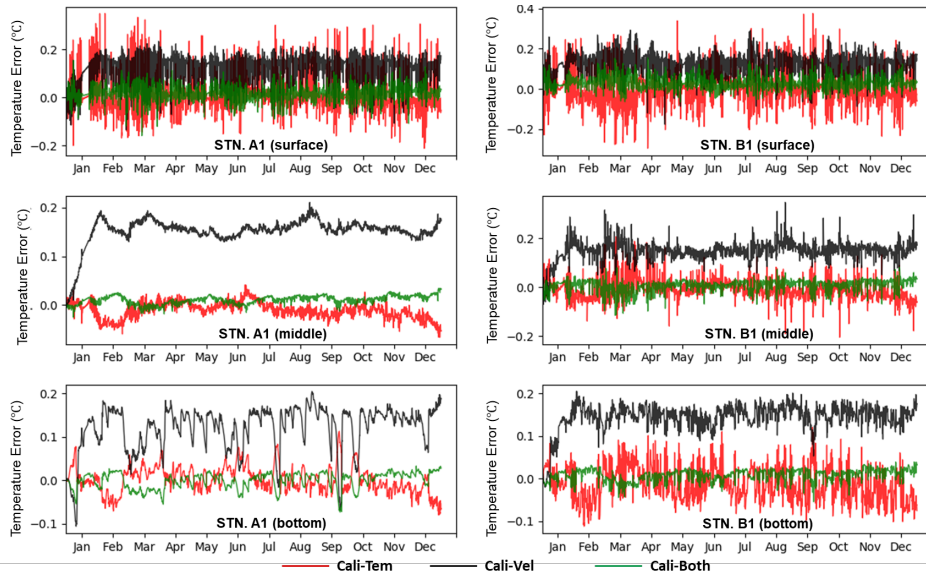


400

401 **Figure 3.** Scatter plot of velocity error  $\Delta \overline{vel}$  in horizontal (X and Y direction) between simulated velocity  
 402  $Sim_{t,j}^{\overline{vel}}(X^*)$  and observed velocity  $Obs_{t,j}^{\overline{vel}}$  at location  $j$ . Each dot denotes the velocity error  $\Delta \overline{vel}$  of location  $j$   
 403 at one time step.  $j$  = surface layer of STN. A1 for upper panel and  $j$  = STN. B1 for lower panel.  $X^*$  is the optimal  
 404 solution found by PODS in each scenario: Cali-Tem (red dots); Cali-Vel (black dots) and Cali-Both (green dots)  
 405 as listed in Table 6. The “True” solution is on or near the intersection of the two perpendicular black lines.

406

Figure 4 shows the temperature error of solutions from three different calibration scenarios: Cali-Tem  
 407 (red time-series), Cali-Vel (black time-series) and Cali-Both scenarios (green time-series). The errors between  
 408 simulated and observed water temperature at the surface, middle and bottom layers of two stations (STN. A1 and  
 409 STN B1) are plotted. In general, the temperature error of the solution in Cali-Both scenario is generally close to  
 410 zero °C for all the layers and stations shown. The solution in Cali-Tem scenario also got temperature error close  
 411 to zero °C at the middle and bottom layer at STN. A1, but it has larger temperature error than solution in Cali-  
 412 Both at surface layer of STN. A1 and all layers of STN. B1. The solution in Cali-Vel scenario generally  
 413 overestimated the water temperature in all locations (i.e., all the surface, middle and bottom layers at both  
 414 stations). The temperature error of solution in Cali-Vel is much larger than solution in Cali-Tem and Cali-Both  
 415 scenarios in the middle and bottom layer of both stations. The temperature error at most times, for the Cali-Vel  
 416 scenario, is greater than 0.1 °C. This might be because both the Stanton and Dalton numbers are underestimated  
 417 in the Cali-Vel scenario when compared with the True solution ( $X^R$ ) (As shown in Table 5). The Dalton number  
 418  $C_e$  affects the evaporative heat flux modeling and the Stanton number  $C_H$  influences the convective heat flux  
 419 modeling in the Delft3D-FLOW model (Hydraulics, 2006). For the solution in Cali-Vel, a smaller Stanton  
 420 number  $C_H$  = (shown in Table 5) might lead to underestimated convective heat flux, which will lead to the  
 421 overestimated of the water temperature. In summary, calibrating to temperature and velocity (i.e., Cali-Both) give  
 422 the best solution in terms of temperature error compare with calibrating to temperature or velocity only (i.e., Cali-  
 423 Tem or Cali-Vel). Calibrating to velocity only (Cali-Vel) gives the worst result in terms of temperature fit.



424  
 425 **Figure 4.** Time-series plots of temperature error  $\Delta T$  between simulated water temperature and  $Sim_{t,j}^{Tem}(X^*)$  and  
 426 observed water temperature ( $Obs_{t,j}^{Tem}$ ) at location  $j$  where  $j =$  surface layer of STN4 for left panel and  $j =$  STN1  
 427 for the right panel.  $X^*$  is the optimal solution found by P-DYCORs in each scenario: Cali-Tem (Red lines); Cali-  
 428 Vel (Black lines) and Cali-Both (green lines) as listed in Table 5.

**Table 5.** The composite error of each variable and the corresponding parameter configuration of the selected  
 optional solution obtained via PODS in three calibration scenarios (Cali-Tem, Cali-Vel and Cali-Both). True  
 solution ( $X^R$ ) defined in Table 2 is given for reference. The parameter symbols are defined in Table 2.

		True Solution ( $X^R$ )	Cali-Tem	Cali-Vel	Cali-Both
Composite error of each variable <sup>1</sup>	$f_{Tem}(X)$	0	0.0202	0.0601	0.0108
	$f_{Vel}(X)$	0	5.1945	2.7390	1.8006
Computed Parameter Vector ( $X^*$ )	$v_H^{back}$ (m <sup>2</sup> /s)	0.5	0.7107	0.5084	0.4516
	$D_H^{back}$ (m <sup>2</sup> /s)	0.5	0.1930	0.8427	0.4562
	$v_V^{back}$ (m <sup>2</sup> /s)	5.00E-05	3.96E-04	3.40E-05	3.00E-05
	$D_V^{back}$ (m <sup>2</sup> /s)	5.00E-05	1.12E-04	6.08E-06	2.98E-05
	$L_{oz}$ (m)	0.015	0.0110	0.0490	0.0340
	$H_{Secchi}$ (m)	1	0.5902	1.4147	1.1358
	$c_p$ (-)	0.0013	0.0017	0.0013	0.0011
	$c_H$ (-)	0.0013	0.0013	0.0012	0.0013
$n$ (m <sup>-1/3</sup> s)	0.022	0.0229	0.0209	0.0243	

<sup>1</sup>Smaller variable errors ( $f_{Tem}(X)$  (see Eq. (7)) and  $f_{Vel}(X)$  (see Eq. (10))) are better, and the variable errors of the true solution  $X^R$  are zero (for both  $f_{Tem}(X)$  and  $f_{Vel}(X)$ ).

429

### 430 3.2 Optimization Search Dynamics under Different Calibration Scenarios

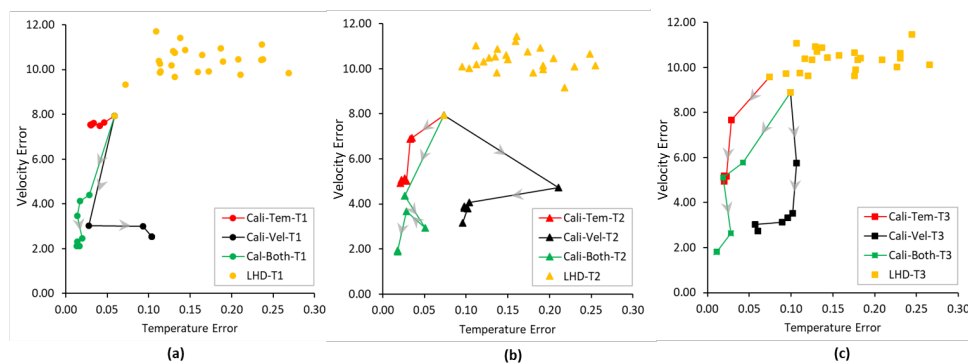
431 We further analyze calibration progress of PODS for Cali-Tem, Cali-Vel and Cali-Both, to understand calibration  
 432 convergence speeds of the three formulations. The purpose of the calibration progress analysis is to visualize the





433 improvement in calibration quality of both temperature and velocity variables from the initial Latin Hypercube  
434 Designs (LHD), for all three formulations.

435 Figure 5 plots the calibration progress of the three formulations (i.e., Cali-Tem, Cali-Vel and Cali-Both)  
436 using PODS. Each subplot within Fig. 5, corresponds to the different concurrent optimization trials (i.e., trials of  
437 the stochastic optimization method using the same initial points from LHD) for each formulation. The best  
438 solutions are near the origin of each graph. Moreover, Fig. 5 plots the progress (quantified by visualizing both  
439 temperature and velocity errors) of the best solution found (measured in terms of the objective function value in  
440 each calibration scenario) during the search. Figure 5 indicates that when calibrating to temperature or velocity  
441 only, the optimization search cannot guarantee the improvement of the fit of another variable. For example, in  
442 Fig. 5 (a), when calibrating to velocity only, the temperature error of the best solution found at the end of the  
443 optimization search stage is worse than the temperature error of the best solution found after initial LHD, even  
444 though there is improvement in terms of velocity fit. Similarly, when calibrating to temperature only, the  
445 improvement on velocity fit is also not significant (for instance, in Fig. 5 (a)). When calibrating to the fit of both  
446 temperature and velocity using the DYN0 formulation, the fit of both temperature and velocity improves in all  
447 trials, and the improvement remains balanced during the optimization search. Figure 5 also indicates that the final  
448 solution found in Cali-Both scenarios dominates the best solution found by PODS in Cali-Tem and Cali-Vel in  
449 terms of both temperature and velocity fit.



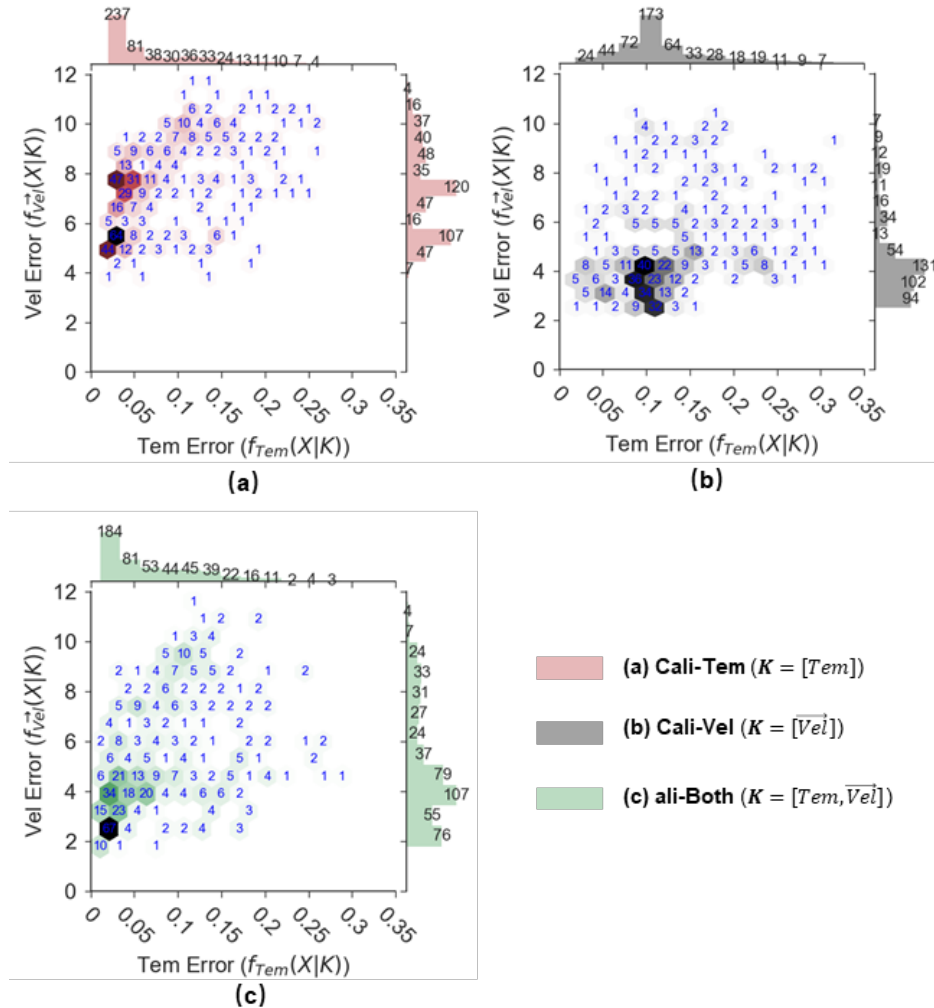
450

451 **Figure 5.** Calibration progress plot of the best solution found (in term of objective function value) during  
452 optimization search by PODS when calibrating to temperature only (Cali-Tem), calibrating to velocity only (Cali-  
453 Vel), and calibrating to both temperature and velocity (Cali-Both). Three random trials (i.e., T1, T2, and T3)  
454 are plotted in (a), (b), and (c). Lower velocity and temperature error are better. The yellow makers are evaluation  
455 point in initial experiment design using Latin Hypercube Design (LHD). Besides solutions in LHD, only the best  
456 solution in each of the optimization iterations are plotted (i.e., makers lined with lines). The line links the best  
457 previous solution in one iteration to the best solution in next iteration. The arrow indicates the direction from the  
458 previous solution to the next solution.

459 It is also important to understand the ‘frequency’ or likelihood with which PODS can find good  
460 temperature and velocity calibrations via the three different formulations proposed in this study. Hence, we also  
461 do a comparative frequency analysis of the errors (for velocity or temperature) of all evaluated points ( $X_i, i =$   
462  $1, \dots, 3 * N_{max}$ ) from all trials (3 trials) of PODS when using difference calibration formulations (see Table 3).  
463 The purpose of this frequency analysis is to understand the likelihood with which the three different formulations  
464 can obtain good velocity and temperature calibrations. The frequency analysis results are presented in Fig. 6 via



465 visualizations of empirical histograms of both velocity error and temperature error (from all solutions of 3 trials  
 466 of PODS) for each calibration scenario.



467  
 468 **Figure 6.** Distribution plot of all the evaluated points found by PODS (over 3 trials) in terms of temperature  
 469 composite error  $f_{Tem}(X|K)$  and velocity composite error  $f_{\overline{Vel}}(X|K)$  in each scenario: Cali-Tem ( $K = [Tem]$ ),  
 470 Cali-Vel ( $K = [\overline{Vel}]$ ), and Cali-Both ( $K = [Tem, \overline{Vel}]$ ). The number inside each hexagon represent the number  
 471 of evaluated points located in that hexagon (e.g. with the combination temperature and velocity error associated  
 472 with the corresponding values on the axes.) Darker color in hexagon means larger number of evaluated points  
 473 located in that hexagon. The bar plot along the upper x axis ( $f_{Tem}(X|K)$ ) are the distribution of the evaluation  
 474 points in terms of temperature error only. The bar plot along y axis ( $f_{\overline{Vel}}(X|K)$ ) are the distribution of the  
 475 evaluation points in terms of velocity error only. The number above the bar shows how many evaluated points  
 476 located in that bin. Smaller error ( $f_{Tem}(X|K)$  or  $f_{\overline{Vel}}(X|K)$ ) is better. The true solution ( $f_{Tem}(X^R|K)$ ,  $f_{\overline{Vel}}(X^R|K)$ )  
 477 is the origin of each subplot.

478 Figure 6 plots the error distribution of all the evaluated points over three trials (576 evaluations) for each  
 479 scenario: Cali-Tem ( $K = [Tem]$ ), Cali-Vel ( $K = [\overline{Vel}]$ ), and Cali-Both ( $K = [Tem, \overline{Vel}]$ ). The different subplots  
 480 in Fig. 6 provide a visualization of the velocity (vertical axis) and temperature (horizontal axis) error distribution



481 via hexagonal bin (hexbin) plots (inside the square) and error histograms (outside the square) for each of the  
 482 calibration scenarios. The number inside each hexbin denotes the number of evaluated points (for that combination  
 483 of temperature error and velocity error) located in that hexbin. Furthermore, the hexbin with a larger number of  
 484 evaluated points is highlighted with a darker color shade. The temperature histogram columns (above the square)  
 485 represents the sum of all the hexbins inside the square directly beneath the number in the column. For velocity  
 486 histogram (on right side of square), the column height depends on the sum of all the hexbins in the row to the left  
 487 of the number.

488 The temperature and error velocity distribution visualizations of Fig. 6 clearly show that calibrating to  
 489 both temperature and velocity data (see Fig. 6 (c), i.e., error distribution for the Cali-Both scenario), provides good  
 490 temperature and velocity calibrations with a higher frequency. Figure 6 (c) shows that it is highly likely that both  
 491 temperature and velocity errors are lower (indicated by darker hexbins with temperature error  $f_{Tem}(\mathbf{X}|\mathbf{K})$  less  
 492 than 0.05 and velocity error  $f_{vel}(\mathbf{X}|\mathbf{K})$  less than 4). Consequently, Fig. 6(c) also illustrates that the newly  
 493 proposed DYNO (see Eq. (3)) works effectively, in this case, to calibrate multiple variables simultaneously.

494 Figure 6 also illustrates that it is better to calibrate the hypothetical hydrodynamic model to velocity data  
 495 rather than temperature data (see Fig. 6(a) and Fig. 6(b)) (if data for both variables is not available). Figure 6(a)  
 496 indicates that calibrating to temperature only (i.e., the Cali-Tem scenario) results in a high chance that velocity  
 497 error would be high (see the velocity error histogram in Fig. 6(a)). However, Fig. 6(b) illustrates that the errors in  
 498 temperature when calibrating to velocity only (Cali-Vel) are likely to be relatively small in magnitude (see the  
 499 temperature error histogram of Fig. 6(b)).

500 From the above discussion, we can conclude that calibrating to both temperature and velocity data with  
 501 the newly proposed DYNO (implemented within the efficient surrogate algorithm PODS) is effective in obtaining  
 502 a balanced calibration of both temperature and velocity variables. In real-world lake hydrodynamic applications,  
 503 if available, both temperature and velocity data should be used for lake hydrodynamic model calibration.  
 504 However, the very common practice of calibrating only to temperature data is shown to be unable to reproduce  
 505 the flow dynamics well. This supports extra effort and expense to collect velocity data is expected to give a  
 506 beneficial effect.

### 507 3.3 Impact of Different Forms of Normalization on the Performance of DYNO

508 This section investigates the impact of using different forms of normalization in the new objective function DYNO  
 509 on optimization search performance. In Eq. (3), the error of each variable is normalized by the maximum and  
 510 minimum values  $f_k^{max}(\mathbf{X})$  and  $f_k^{min}(\mathbf{X})$  of  $f_k(\mathbf{X})$  among all the evaluations evaluated so far. One concern of  
 511 using the maximum value  $f_k^{max}(\mathbf{X})$  is that the objective function can be affected by extremely bad evaluations  
 512 points. Another approach is to use the median value  $f_k^{median}(\mathbf{X})$  of  $f_k(\mathbf{X})$  among all the evaluations evaluated so  
 513 far as a replacement of  $f_k^{max}(\mathbf{X})$  to normalize the error of each variable. We refer to DYNO using the median  
 514 value  $f_k^{median}(\mathbf{X})$  as DYNO-N2 (as shown in Eq. (13)) to differentiate it from DYNO using the maximum value  
 515  $f_k^{max}(\mathbf{X})$  (as shown in Eq. (3)), which we refer to as DYNO-N1 in the following text.

$$516 F(\mathbf{X}|\mathbf{K}) = \sum_{k \in K} \frac{f_k(\mathbf{X}) - f_k^{min}(\mathbf{X})}{f_k^{median}(\mathbf{X}) - f_k^{min}(\mathbf{X})} \quad (13)$$

$$517 f_k^{median}(\mathbf{X}) = \text{med} \{f_k(\mathbf{X}) \text{ for all } \mathbf{X} \in \psi\} \quad (14)$$

518

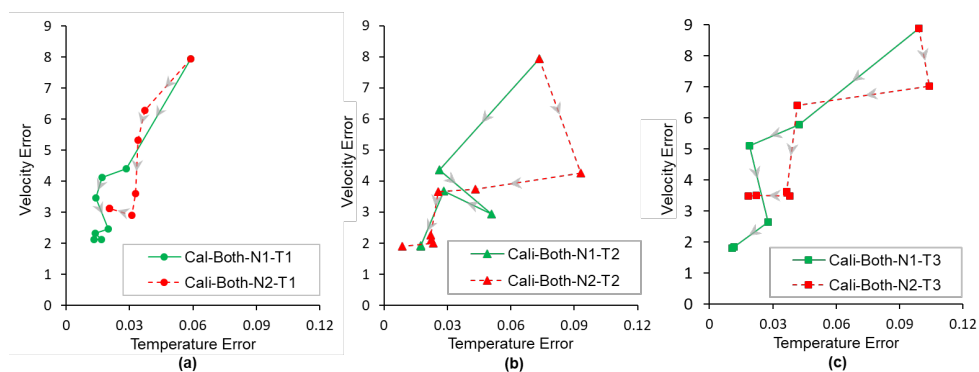


519 where  $f_k^{median}(\mathbf{X})$  and  $f_k^{min}(\mathbf{X})$  are the median and minimum values of  $f_k(\mathbf{X})$  among all the evaluations  
520 evaluated so far, and hence they are updated dynamically in each iteration during optimization.

521 The implementation of DYNO-N2 is similar to the implementation of DYNO-N1 (Eq. (3)). The only  
522 change is replacing the calculation related to  $f_k^{max}(\mathbf{X})$  with  $f_k^{median}(\mathbf{X})$ . We tested relative efficacies of DYNO-  
523 N1 and DYNO-N2, by comparing three calibration trials, of each DYNO variant (using PODS), where each  
524 concurrent calibration trial was initialized using the same LHD. Figure 7 shows the progress of PODS with the  
525 two forms of DYNO as the objective functions. Figure 7 is similar in design to Fig. 5, and indicates that both  
526 forms of DYNO are able to balance the calibration on temperature and velocity. There are two trials where PODS  
527 with DYNO-N1 (using  $f_k^{max}(\mathbf{X})$  for normalization) found a better solution than PODS with DYNO-N2 (using  
528  $f_k^{median}(\mathbf{X})$  for normalization).

529 The results here indicate that DYNO-N1 seems not adversely affected by the bad solution. A reason for  
530 this may be that PODS typically do not generate extremely bad solutions (i.e., outlier solutions with extremely  
531 large errors), since algorithm search is concentrated around the best solution found so far. However, if other  
532 optimization algorithms are used for calibration especially algorithms that explore the search space more, there  
533 maybe a higher likelihood of encountering outlier /extremely bad solutions during optimization search.  
534 Consequently, the performance of such algorithm with DYNO-N2 might be better than with DYNO-N2, which  
535 might need further investigation. The outlier solutions here mean solutions (obtained during the optimization  
536 search phase) that have much larger errors than other solutions found so far. Outlier or extremely bad solutions  
537 are also like for calibration problems where the model output is very sensitive to the calibration parameters (i.e.,  
538 a small change in model parameters can cause huge changes in the model output that leads to much worse  
539 solutions).

540



541

542

543 **Figure 7.** Calibration progress plot in terms of the best solution found during optimization search when using  
544 DYNO-N1 and DYNO-N2 as the objective function. Three random trials (T1, T2, and T3) are plotted in (a), (b),  
545 and (c). Lower velocity and temperature error are better. Figure 7 uses the same format as Figure 5.

#### 546 3.4 Value of Velocity Measures in 3D Lake Model Calibration

547 High quality hydrodynamic simulations (e.g., thermal structure, current velocities, flow advection and vertical  
548 mixing) are vital for accurate spatial modelling of water quality in lakes. The hydrodynamic process influences  
549 the transport & production or transformation of biological and chemical components. Hence, if the simulation of



550 flow dynamics is not adequately accurate, there is no way to achieve accuracy in the simulation of water quality.  
551 Previous studies use mostly temperature observations for the 3D lake hydrodynamic model calibration. Whereas,  
552 velocity data is less commonly used compared with temperature data for model calibration.

553 Our results in section 3.1 indicate that calibrating to temperature data only cannot guarantee accuracy in  
554 velocity simulation. Not using velocity data in model calibration (i.e., using temperature data in model calibration  
555 only) thus, may lead to large velocity errors (as indicated in the Figure 3). The inclusion of velocity measurements  
556 in calibration not only reduces velocity error but also helps improving the temperature fit. For example, in Fig. 4,  
557 when calibrating to both temperature and velocity data, the temperature error is smaller than the temperature error  
558 when calibrating to temperature data only. This is most obvious in the surface layers of both STN. A1 and STN.  
559 B1, where the temperature error when calibrating to both temperature and velocity (i.e., Cali-Both) is much  
560 smaller compared to calibrating to temperature only (i.e., Cali-Vel). The better result (better fit of temperature as  
561 well as velocity) in Cali-Both demonstrates the effectiveness of using velocity measures in 3D hydrodynamic lake  
562 model calibration. The comparison of calibrated parameter values in Cali-Both and Cali-Tem scenarios (in Table  
563 5) also demonstrates the value of using velocity data besides temperature data in model calibration. In Table 5,  
564 we can see that the calibrated value of viscosity and diffusivity parameters in Cali-Both is much closer to the true  
565 value than that in Cali-Tem. This shows that the use of velocity measures helps to improve the calibrate of these  
566 viscosity and diffusivity parameters.

567 The risk of using only temperature data without velocity data, even for accurately simulating water  
568 temperature, is that temperature simulation is affected by both the flow dynamics and the heat transfer process.  
569 The fit of temperature data is a result of the combination of these two processes. However, the fit of the  
570 temperature data cannot guarantee accurate simulation of each of the processes, though accurate simulation of  
571 each process does guarantee the fit of temperature data. The velocity observation hence is valuable to help improve  
572 the flow dynamics simulation of the model, which is not only important for temperature simulation but also other  
573 water quality substances simulation (e.g., these biological and chemical components). Our research implication  
574 of the use of velocity observations is also in line with the study of Baracchini et al. (2020), where they also suggest  
575 have both temperature and current velocity for a complete system calibration.

### 576 3.5 Possibilities for Other Applications

577 In this study, we only demonstrate how DYNO can be incorporated into PODS parallel surrogate global  
578 optimization algorithm. (see section 2.6). However, the new objective function DYNO could also be easily  
579 utilized with other heuristic optimization methods (e.g., serial or parallel versions of Genetic Algorithm (Davis,  
580 1991) and Differential Evolution (Tasoulis et al., 2004)) for effectively calibrating other multi-variables  
581 calibration problems. We have not provided a precise methodology for incorporating DYNO into other  
582 optimization methods though, since incorporation of DYNO depends on the structure of an optimization method,  
583 and structures of optimization methods vary a lot. We did illustrate in section 2.6 and Figure 3 on how components  
584 of parallel PODS are modified in order to use DYNO. Other optimization methods could be modified in a similar  
585 way to incorporate DYNO for use in multi-variable calibration.

586 Also, there are numerous other model calibration paradigms in general hydrology and water resources  
587 (besides the hydrodynamic model calibration) where simultaneous multi-variable and multi-site calibrations are  
588 required. Some examples of such multi-variable & multi-site calibration problems include watershed model



589 calibration (Franco et al., 2020; Odusanya et al., 2019), seawater intrusion model calibration (Coulon et al., 2021),  
590 and water quality model calibration (Xia and Shoemaker, 2021) etc. In these problems, there are usually multiple  
591 constituents (e.g., substances) to be calibrated and the observations are usually available at multiple locations. Our  
592 new DYNO can potentially be used to calibrate them simultaneously. A popular calibration strategy for such  
593 problems in general hydrology is to use multi-objective calibration where it is assumed that a trade-off exists  
594 between multiple hydrologic responses (e.g., high flow, low flow, water balance, water quality etc.).

595 Using multi-objective algorithms, however, for calibrating hydrologic and watershed quality models may  
596 not be the most suited strategy for some case studies because i) multi-objective calibration can be computationally  
597 intensive if underlying simulations are computationally expensive and ii) meaningful trade-offs between different  
598 objectives may not exist. Kollat et al. (2012) demonstrate that prior multi-objective calibration exercises may have  
599 over-reported the number of meaningful trade-offs in hydrologic model calibration. DYNO is a reasonable  
600 alternative to classical multi-objective calibration in calibration problems where the trade-off between multiple  
601 component calibration objectives is not significant, because i) a balance between multiple constituent objectives  
602 is maintained with DYNO and ii) a single objective algorithm can be used with DYNO, which is computationally  
603 more efficient than a multi-objective algorithm. This is especially true for multi-constituent watershed model  
604 calibration problems where the achievable objective functions ranges for different constituents (e.g., flow,  
605 sediment, phosphorus etc.) are quite different. Multiple prior studies (Moriassi et al., 2012; Moriassi et al., 2015)  
606 highlight that achievable ranges of statistical calibration measures (e.g., Nash Sutcliffe Efficiency (NSE), bias  
607 etc.) are significantly different for different constituents (e.g., streamflow, sediment, total phosphorus etc.).  
608 Moriassi et al. (2015) note that in most watershed model case studies, the achievable range of NSE for streamflow  
609 is higher than the achievable range for total phosphorus. Hence, DYNO may be extremely effective in balancing  
610 simultaneous calibration of streamflow and phosphorus for such case studies. We believe that there is immense  
611 potential in the application of DYNO for multi-constituent watershed model calibration.

#### 612 **4 Conclusions**

613 We conclude that the Dynamically Normalized Objective Function we propose is a new effective way to balance  
614 the calibration to different variables (i.e., temperature and velocity) in optimization-based -calibration. It is  
615 possible that the magnitudes of goodness-of-fit measures for different variables are very different (which may  
616 fluctuate during the optimization search), and thus the optimization search cannot maintain balance between  
617 different variables. Hence DYNO dynamically modifies the objective function, for multi-variable calibration, so  
618 that the error for each variable is being dynamically normalized in each iteration. This is to ensure that the search  
619 is giving approximately equal weight to each variable (e.g., velocity and temperature).

620 The proposed DYNO is tested in this study for simultaneous temperature and velocity calibration of a  
621 lake model. Moreover, DYNO is integrated with the PODS algorithm for testing on expensive lake hydrodynamic  
622 model calibration in parallel. Results indicate that using DYNO ensures a balanced calibration between  
623 temperature and velocity. We provide a detailed analysis to illustrate that DYNO balances the weight between  
624 different objectives dynamically, and thus allows for a balanced parameter search during optimization.

625 We conclude that calibrating to the error of one variable (either temperature or velocity) cannot guarantee  
626 the goodness-of-fit of another variable. Of course, the most accurate predications can be obtained by having both  
627 temperature and velocity data. These comparisons are possible because we have, via synthetic simulation, the true



628 solution for the lake model. Our analysis suggests that in real practice, both temperature and velocity data are  
629 important for model calibration. The common practice of calibrating only to temperature data is not sufficient to  
630 reproduce the flow dynamics accurately and extra effort and expense to collect velocity data is expected to give a  
631 beneficial effect.

632 There are many possible future areas for application of this method. The Dynamically Normalized  
633 objective function (DYNO) would be effective for other multi-variable and multi-site calibration problems  
634 (especially for problems with many variables). Future research could apply the DYNO methods on other problems  
635 and using other optimization algorithms.

#### 636 **Code and Data availability**

637 The tropical reservoir hydrodynamic numerical model and data were provided by PUB, Singapore's National  
638 Water Agency (<https://www.pub.gov.sg/>). The Delft3D open source code could be downloaded from  
639 <https://oss.deltares.nl/web/delft3d/source-code>. The PODS open source code could be download from  
640 <https://github.com/louisXW/PODS>. The code for objective function can be download from  
641 <https://github.com/louisXW/DYNO-pods>.

#### 642 **Author contributions**

643 WX took responsibility for the methodology, software, formal analysis, investigation, original draft preparation,  
644 and visualization. WX, TA, CAS discussed the design and results and edited the manuscript.

#### 645 **Competing interests**

646 The authors declare that they have no conflict of interest.

#### 647 **Acknowledgments**

648 This research was supported by the National Research Foundation, Prime Minister's Office, Singapore under its  
649 Campus for Research Excellence and Technological Enterprise (CREATE) programme and from Professor  
650 Shoemaker's start-up grant from the National University of Singapore (NUS). The authors acknowledge PUB,  
651 Singapore's National Water Agency for providing the tropical reservoir hydrodynamic numerical model and data.  
652 The computational work for this article was entirely performed on resources of the National Supercomputing  
653 Centre, Singapore (<https://www.nscg.sg>).

#### 654 **References**

- 655 Afshar, A., Kazemi, H., and Saadatpour, M.: Particle swarm optimization for automatic calibration of large scale  
656 water quality model (CE-QUAL-W2): Application to Karkheh Reservoir, Iran, *Water Resources*  
657 *Management*, 25, 2613-2632, 2011.
- 658 Afshar, A., Shojaei, N., and Sagharjooghifarahani, M.: Multiobjective calibration of reservoir water quality  
659 modeling using multiobjective particle swarm optimization (MOPSO), *Water resources management*, 27,  
660 1931-1947, 2013.
- 661 Akhtar, T. and Shoemaker, C. A.: Multi objective optimization of computationally expensive multi-modal  
662 functions with RBF surrogates and multi-rule selection, *Journal of Global Optimization*, 64, 17-32, 2016.
- 663 Alfonso, L., Jonoski, A., and Solomatine, D.: Multiobjective optimization of operational responses for  
664 contaminant flushing in water distribution networks, *Journal of Water Resources Planning and Management*,  
665 136, 48-58, 2010.





- 666 Ayala, A. I., Moras, S., and Pierson, D. C.: Simulations of future changes in thermal structure of Lake Erken:  
667 proof of concept for ISIMIP2b lake sector local simulation strategy, *Hydrology and Earth System Sciences*,  
668 24, 3311-3330, 2020.
- 669 Baracchini, T., Hummel, S., Verlaan, M., Cimatoribus, A., Wüest, A., and Bouffard, D.: An automated calibration  
670 framework and open source tools for 3D lake hydrodynamic models, *Environmental Modelling & Software*,  
671 134, 104787, 2020.
- 672 Bartz-Beielstein, T. and Zaefferer, M.: Model-based methods for continuous and discrete global optimization,  
673 *Applied Soft Computing*, 55, 154-167, 2017.
- 674 Beletsky, D., Schwab, D., and McCormick, M.: Modeling the 1998–2003 summer circulation and thermal  
675 structure in Lake Michigan, *Journal of Geophysical Research: Oceans*, 111, 2006.
- 676 Chanudet, V., Fabre, V., and van der Kaaij, T.: Application of a three-dimensional hydrodynamic model to the  
677 Nam Theun 2 Reservoir (Lao PDR), *Journal of Great Lakes Research*, 38, 260-269, 2012.
- 678 Coulon, C., Pryet, A., Lemieux, J.-M., Yrro, B. J. F., Bouchedda, A., Gloaguen, E., Comte, J.-C., Dupuis, J. C.,  
679 and Banton, O.: A framework for parameter estimation using sharp-interface seawater intrusion models,  
680 *Journal of Hydrology*, 600, 126509, 2021.
- 681 Davis, L.: *Handbook of genetic algorithms*, 1991.
- 682 Deltares: *Delft3D-FLOW user manual*, Deltares, Delft, the Netherlands 2014.
- 683 Elhakeem, A., Elshorbagy, W., and Bleninger, T.: Long-term hydrodynamic modeling of the Arabian Gulf,  
684 *Marine Pollution Bulletin*, 94, 19-36, 2015.
- 685 Fabio, P., Aronica, G. T., and Apel, H.: Towards automatic calibration of 2-D flood propagation models,  
686 *Hydrology and Earth System Sciences*, 14, 911-924, 2010.
- 687 Franco, A. C. L., Oliveira, D. Y. d., and Bonumá, N. B.: Comparison of single-site, multi-site and multi-variable  
688 SWAT calibration strategies, *Hydrological Sciences Journal*, 65, 2376-2389, 2020.
- 689 Galelli, S., Castelletti, A., and Goedbloed, A.: High-Performance Integrated Control of water quality and quantity  
690 in urban water reservoirs, *Water Resources Research*, 51, 9053-9072, 2015.
- 691 Gaudard, A., Schwefel, R., Vinná, L. R., Schmid, M., Wüest, A., and Bouffard, D.: Optimizing the  
692 parameterization of deep mixing and internal seiches in one-dimensional hydrodynamic models: a case study  
693 with Simstrat v1. 3, *Geoscientific Model Development*, 10, 3411-3423, 2017.
- 694 Giuliani, M., Castelletti, A., Pianosi, F., Mason, E., and Reed, P. M.: Curses, tradeoffs, and scalable management:  
695 Advancing evolutionary multiobjective direct policy search to improve water reservoir operations, *Journal of*  
696 *Water Resources Planning and Management*, 142, 04015050, 2016.
- 697 Gupta, H. V., Kling, H., Yilmaz, K. K., and Martinez, G. F.: Decomposition of the mean squared error and NSE  
698 performance criteria: Implications for improving hydrological modelling, *Journal of hydrology*, 377, 80-91,  
699 2009.
- 700 Haftka, R. T., Villanueva, D., and Chaudhuri, A.: Parallel surrogate-assisted global optimization with expensive  
701 functions—a survey., *Structural Multidisciplinary Optimization*, 54, 3-13, 2016.
- 702 Herman, J. D., Zeff, H. B., Reed, P. M., and Characklis, G. W.: Beyond optimality: Multistakeholder robustness  
703 tradeoffs for regional water portfolio planning under deep uncertainty, *Water Resources Research*, 50, 7692-  
704 7713, 2014.
- 705 Huang, A., Rao, Y. R., Lu, Y., and Zhao, J.: Hydrodynamic modeling of Lake Ontario: An intercomparison of  
706 three models, *Journal of Geophysical Research: Oceans*, 115, 2010.
- 707 Hui, Y., Zhu, Z., and Atkinson, J. F.: Mass balance analysis and calculation of wind effects on heat fluxes and  
708 water temperature in a large lake, *Journal of Great Lakes Research*, 44, 1293-1305, 2018.
- 709 Hydraulics, D.: *Delft3D-FLOW user manual*, Delft, the Netherlands, 2006.
- 710 Jin, K.-R., Hamrick, J. H., and Tisdale, T.: Application of three-dimensional hydrodynamic model for Lake  
711 Okeechobee, *Journal of Hydraulic Engineering*, 126, 758-771, 2000.
- 712 Kaçkoç, M. and Beyhan, M.: Hydrodynamic and water quality modeling of Lake Eğirdir, *Clean–Soil, Air, Water*,  
713 42, 1573-1582, 2014.
- 714 Kollat, J. B., Reed, P. M., and Wagener, T.: When are multiobjective calibration trade-offs in hydrologic models  
715 meaningful?, *Water Resources Research*, 48, W03520, 2012.
- 716 Lu, D., Ricciuto, D., Stoyanov, M., and Gu, L.: Calibration of the E3SM land model using surrogate-based global  
717 optimization, *Journal of Advances in Modeling Earth Systems*, 10, 1337-1356, 2018.
- 718 Luo, L., Hamilton, D., Lan, J., McBride, C., and Trolle, D.: Autocalibration of a one-dimensional hydrodynamic-  
719 ecological model (DYRESM 4.0-CAEDYM 3.1) using a Monte Carlo approach: simulations of hypoxic  
720 events in a polymictic lake, *Geoscientific Model Development*, 11, 903-913, 2018.
- 721 Marti, C. L., Mills, R., and Imberger, J.: Pathways of multiple inflows into a stratified reservoir: Thomson  
722 Reservoir, Australia, *Advances in water resources*, 34, 551-561, 2011.
- 723 Moriasi, D. N., Arnold, J. G., Van Liew, M. W., Bingner, R. L., Harmel, R. D., & Veith, T. L.: Model evaluation  
724 guidelines for systematic quantification of accuracy in watershed simulations, *Transactions of the*  
725 *ASABE*, 50, 885-900, 2012.



- 726 Moriasi, D. N., Gitau, M. W., Pai, N. and Daggupati, P.: Hydrologic and water quality models: Performance  
727 measures and evaluation criteria, *Transactions of the ASABE*, 58, 1763-1785, 2015.
- 728 Odusanya, A. E., Mehdi, B., Schürz, C., Oke, A. O., Awokola, O. S., Awomeso, J. A., Adejuwon, J. O., and  
729 Schulz, K.: Multi-site calibration and validation of SWAT with satellite-based evapotranspiration in a data-  
730 sparse catchment in southwestern Nigeria, *Hydrology and Earth System Sciences*, 23, 1113-1144, 2019.
- 731 Parsapour-Moghaddam, P. and Rennie, C. D.: Calibration of a 3D hydrodynamic meandering river model using  
732 fully spatially distributed 3D ADCP velocity data, *Journal of hydraulic engineering*, 144, 04018010, 2018.
- 733 Paturi, S., Boegman, L., Bouffard, D., and Rao, Y. R.: Three-dimensional simulation of Lake Ontario North-Shore  
734 hydrodynamics and contaminant transport, *Journal of Hydraulic Engineering*, 141, 04014082, 2014.
- 735 Pelletier, G. J., Chapra, S. C., and Tao, H.: QUAL2Kw—A framework for modeling water quality in streams and  
736 rivers using a genetic algorithm for calibration, *Environmental Modelling & Software*, 21, 419-425, 2006.
- 737 Pijcke, G.: Water quality modelling for Gardens by the Bay, Singapore, National University of Singapore, 2014.
- 738 Råman Vinnå, L., Wüest, A., and Bouffard, D.: Physical effects of thermal pollution in lakes, *Water Resources*  
739 *Research*, 53, 3968–3398, 2017.
- 740 Razavi, S., Tolson, B. A., and Burn, D. H.: Review of surrogate modeling in water resources, *Water Resources*  
741 *Research*, 48, W07401, 2012.
- 742 Reed, P. M., Hadka, D., Herman, J. D., Kasprzyk, J. R., and Kollat, J. B.: Evolutionary multiobjective optimization  
743 in water resources: The past, present, and future, *Advances in water resources*, 51, 438-456, 2013.
- 744 Regis, R. G. and Shoemaker, C. A.: A stochastic radial basis function method for the global optimization of  
745 expensive functions, *INFORMS Journal on Computing*, 19, 497-509, 2007.
- 746 Regis, R. G. and Shoemaker, C. A.: Parallel stochastic global optimization using radial basis functions, *INFORMS*  
747 *Journal on Computing*, 21, 411-426, 2009.
- 748 Regis, R. G. and Shoemaker, C. A.: Combining radial basis function surrogates and dynamic coordinate search in  
749 high-dimensional expensive black-box optimization, *Engineering Optimization*, 45, 529-555, 2013.
- 750 Solomatine, D. P., Dibike, Y. B., and Kukuric, N.: Automatic calibration of groundwater models using global  
751 optimization techniques, *Hydrological Sciences Journal*, 44, 879-894, 1999.
- 752 Soullignac, F., Vinçon-Leite, B., Lemaire, B. J., Martins, J. R. S., Bonhomme, C., Dubois, P., Mezemate, Y.,  
753 Tchiguirinskaia, I., Schertzer, D., and Tassin, B.: Performance Assessment of a 3D Hydrodynamic Model  
754 Using High Temporal Resolution Measurements in a Shallow Urban Lake, *Environmental Modeling &*  
755 *Assessment*, 22, 309-322, 2017.
- 756 Tasoulis, D. K., Pavlidis, N. G., Plagianakos, V. P., and Vrahatis, M. N.: Parallel differential evolution,  
757 *Proceedings of the 2004 Congress on Evolutionary Computation (IEEE Cat. No. 04TH8753)*, 2023-2029,
- 758 Tolson, B. A. and Shoemaker, C. A.: Dynamically dimensioned search algorithm for computationally efficient  
759 watershed model calibration, *Water Resources Research*, 43, 2007.
- 760 Uittenbogaard, R. E., Van Kester, J. T. M., and Stelling, G. S.: Implementation of Three Turbulence Models in  
761 TRISULA for Rectangular Horizontal Grids: Including 2DV-testcases, *Delft Hydraulics*1992.
- 762 Wagner, C. R. and Mueller, D. S.: Use of velocity data to calibrate and validate two-dimensional hydrodynamic  
763 models, *Proceedings of the Second Federal Interagency Hydrologic Modeling Conference*,
- 764 Wahl, B. and Peeters, F.: Effect of climatic changes on stratification and deep-water renewal in Lake Constance  
765 assessed by sensitivity studies with a 3D hydrodynamic model, *Limnology and Oceanography*, 59, 1035-  
766 1052, 2014.
- 767 Wilson, H. L., Ayala, A. I., Jones, I. D., Rolston, A., Pierson, D., de Eyto, E., Grossart, H.-P., Perga, M.-E.,  
768 Woolway, R. I., and Jennings, E.: Variability in epilimnion depth estimations in lakes, *Hydrology and Earth*  
769 *System Sciences*, 24, 5559-5577, 2020.
- 770 Xia, W. and Shoemaker, C.: GOPS: efficient RBF surrogate global optimization algorithm with high dimensions  
771 and many parallel processors including application to multimodal water quality PDE model calibration,  
772 *Optimization and Engineering*, 22, 2741-2777, 10.1007/s11081-020-09556-1, 2021.
- 773 Xia, W., Shoemaker, C., Akhtar, T., and Nguyen, M.-T.: Efficient Parallel Surrogate Optimization Algorithm and  
774 Framework with Application to Parameter Calibration of Computationally Expensive Three-dimensional  
775 Hydrodynamic Lake PDE Models, *Environmental Modelling & Software*, 104910,  
776 <https://doi.org/10.1016/j.envsoft.2020.104910>, 2021.
- 777 Xu, C., Zhang, J., Bi, X., Xu, Z., He, Y., and Gin, K. Y.-H.: Developing an integrated 3D-hydrodynamic and  
778 emerging contaminant model for assessing water quality in a Yangtze Estuary Reservoir, *Chemosphere*, 188,  
779 218-230, 2017.
- 780 Xue, P., Schwab, D. J., and Hu, S.: An investigation of the thermal response to meteorological forcing in a  
781 hydrodynamic model of Lake Superior, *Journal of Geophysical Research: Oceans*, 120, 5233-5253, 2015.
- 782